Reduced Order Models of On-chip Passive Components and Interconnects, Workbench and Test Structures

Daniel Ioan and Gabriela Ciuprina

Politehnica University of Bucharest, Romania lmn@lmn.pub.ro

1 Extraction of the EM-FW State Models for Passive Components

The models of passive components have to describe all relevant electromagnetic field effects at high frequency encountered inside these devices. These effects are quantified by the Maxwell equations of the electromagnetic field in full wave (FW) regime. Therefore, at the first level of approximation, the model of a passive device is defined by an electromagnetic (EM) field problem, formulated by Maxwell partial differential equations with appropriate boundary and initial conditions. This problem defines a consistent I/O system which has a unique response, described by the output signals, for any input signal applied as terminal excitations. This system with distributed parameters has an infinite dimension state space, but a finite number of inputs and outputs related to the device terminals.

The next level of approximation in the modeling process (Fig. 1) results by applying a numerical method to discretize the continuous model defined above. This step associates a simpler ODE to the original PDE model, actually a system of DAE. It is an important step ahead, reducing the infinite dimensional state-space which is specific to distributed systems to a finite one. However, the size of the state-space is still too large for the designers needs. It has an order similar to the number of DOFs associated to the cells, finite elements used to discretize the computational domain.

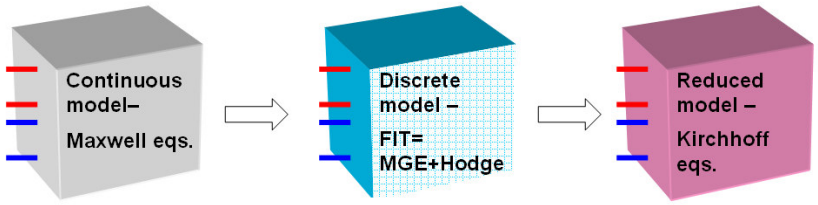

Fig. 1. Three levels of abstraction for a component model and its corresponding equations.

That is why a third step is necessary (Fig. 1), aiming to reduce this order, and to generate a "compact" model, e.g. a small SPICE circuit, which preserves the behaviour of the passive component, from terminals point of view, for instance the input-output relationship.

The basic equations used to model the electromagnetic field effects in any device without movement, including the integrated passive devices are the **Maxwell equations**:

$$\operatorname{curl}\mathbf{H} = \mathbf{J} + \frac{\partial \mathbf{D}}{\partial t}, \tag{1}$$

$$\operatorname{curl}\mathbf{E} = -\frac{\partial \mathbf{B}}{\partial t}, \tag{2}$$

$$\operatorname{div}\mathbf{D} = \rho, \tag{3}$$

$$\operatorname{div}\mathbf{B} = 0. \tag{4}$$

These equations have to be complemented with the constitutive equations, which describe the material behaviour, from electromagnetic point of view. In the linear and isotropic materials, these constitutive equations have the simplest form:

$$\mathbf{D} = \varepsilon\mathbf{E}, \tag{5}$$

$$\mathbf{B} = \mu\mathbf{H}, \tag{6}$$

$$\mathbf{J} = \sigma\mathbf{E}. \tag{7}$$

The three material "constants" have nonnegative values, dependent on position: $\varepsilon(M)$, $\mu(M)$ and $\sigma(M)$. Usually, these functions are constant on sub-domains, separated by discontinuity interfaces between homogeneous materials. The solutions of these equations are the following "fields": $\mathbf{E}(M,t)$, $\mathbf{D}(M,t)$, $\mathbf{B}(M,t)$, $\mathbf{H}(M,t)$, $\mathbf{J}(M,t)$, $\rho(M,t)$, vector or scalar functions of position (M) and time (t). The correct formulation of the continuous field problem (1)÷(7) consists of the identification of the appropriate boundary conditions able to allow the consistent field-circuit coupling. To conclude, the extraction of reduced order models for passive components requires the solution of the correct formulated EM field problem, particularly associated to the concept of Electric Circuit Element defined below [IM99].

An **Electric Circuit Element** *(ECE) is a simply connected domain bounded by a fixed surface Σ comprising n' disjoint parts $S'_1, S'_2, \ldots S'_n$, called electric terminals on which:*

$$\mathbf{n}\cdot\operatorname{curl}\mathbf{E}(P,t) = 0 \quad \text{for } (\forall)\, P \in \Sigma, \tag{8}$$

$$\mathbf{n}\cdot\operatorname{curl}\mathbf{H}(P,t) = 0 \quad \text{for } (\forall)\, P \in \Sigma - \cup S'_k, \tag{9}$$

$$\mathbf{n}\times\mathbf{E}(P,t) = \mathbf{0} \qquad \text{for } (\forall)\, P \in \cup S'_k, \tag{10}$$

where $\mathbf{n}$ *is the normal unitary vector of Σ in the point P (Fig. 2).*

Condition (8) **interdicts the inductive couplings** through the device boundary, between the domain and its environment. Condition (9) **interdicts the conductive and capacitive couplings** through the device boundary, excepting for the electric

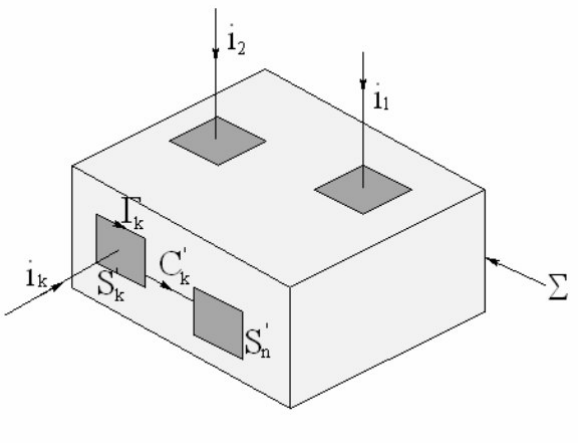

Fig. 2. ECE - Electric Circuit Element with multiple terminals.

terminals. Condition (10) **interdicts the variation of the electric potential over every electric terminal**, allowing the connection of the ECE terminals to the nodes of any external electric circuit. With these boundary conditions, the interaction between ECE and the environment is completely described by $2n'$ scalar variables, two for each terminal: one current and one voltage.

• For each electric terminal k, its **current** is defined as the total current (conduction and displacement) flowing through it:

$$i_k(t) = \int_{\Gamma_k} \mathbf{H} \cdot \mathrm{d}\mathbf{r}, \tag{11}$$

where $\Gamma_k = \partial S'_k$ is a closed curve, the boundary of the terminal surface S'_k. We assume that Γ_k are oriented so that associated normal $\mathbf{n}$ of S'_k is inwards oriented. Due to (9), the sum of all terminal currents is zero and KCL is a consequence.

• For each electric terminal k, its **voltage** is defined as the integral

$$v_k(t) = \int_{C_k} \mathbf{E} \cdot \mathrm{d}\mathbf{r} \tag{12}$$

along an arbitrary curve C_k, included in Σ which is a path between a point on S'_k and a point on a reference terminal, let's say S'_n. The condition (8) ensures the consistent definition of the terminal voltage, its independence from the shape of C_k and KVL as a consequence. The following uniqueness theorem is fundamental for the correct formulation of the EM field problem with appropriate boundary conditions for the models extraction [RTT66].

The electromagnetic power transferred by any ECE through its boundary from outside to inside of it is given by the expression

$$P = \sum_{k=1}^{n'-1} v_k i_k. \tag{13}$$

As a consequence, the EM field problem associated to an ECE with equations (1)÷(7), boundary conditions (8) ÷ (10), zero initial conditions, having some terminals excited by known voltages and the rest by known currents has a unique field solution: $\mathbf{E}(M,t)$, $\mathbf{D}(M,t)$, $\mathbf{B}(M,t)$, $\mathbf{H}(M,t)$, $\mathbf{J}(M,t)$, $\rho(M,t)$, *for* $(\forall)M \in D$, $t > 0$, *and therefore ECE has a unique response for a given arbitrary terminal excitations.*

2 Finite States Representation by Finite Integrals Technique

The Manhattan geometry, characteristic to IC layout makes the Finite Integration Technique (FIT) a suitable numerical method for electromagnetic field computation in that kind of structures. FIT is a numerical method able to solve field problems based on spatial discretization "without shape functions". Two staggered orthogonal (Yee type) grids are used as discretization mesh [CW01]. The centers of the primary cells are the nodes of the secondary cells and the secondary grid is not extended outside the primary grid. The degrees of freedom used by FIT are not local field components as in FEM or in FDTD, but the global variables i.e. electric and magnetic voltages $\mathbf{u}_e$, $\mathbf{u}_m$ and magnetic and electric fluxes $\boldsymbol{\varphi}$, $\boldsymbol{\psi}$ assigned to the grid elements: edges and faces, respectively. They are associated to these grids elements in a coherent manner (Fig. 3). Applying the global form of electromagnetic field equations on the mesh elements (elementary faces and their borders), a system of DAE, called Maxwell Grid Equations (MGE) is obtained:

$$\operatorname{curl}\mathbf{E} = -\frac{\partial \mathbf{B}}{\partial t} \quad \Rightarrow \quad \int_{\Gamma} \mathbf{E}\cdot \mathrm{d}\mathbf{r} = -\iint_{S_\Gamma} \frac{\partial \mathbf{B}}{\partial t}\cdot \mathbf{dA} \quad \Rightarrow \mathbf{C}\mathbf{u}_e = -\frac{\mathrm{d}\boldsymbol{\varphi}}{\mathrm{d}t} \tag{14}$$

$$\hookrightarrow \operatorname{div}\mathbf{B} = 0 \quad \Rightarrow \quad \iint_{\Sigma} \mathbf{B}\cdot \mathbf{dA} = 0 \quad \Rightarrow \quad \mathbf{D}'\boldsymbol{\varphi} = \mathbf{0} \tag{15}$$

$$\operatorname{curl}\mathbf{H} = \mathbf{J} + \frac{\partial \mathbf{D}}{\partial t} \Rightarrow \int_{\Gamma} \mathbf{H}\cdot \mathrm{d}\mathbf{r} = \iint_{S_\Gamma} \left(\mathbf{J} + \frac{\partial \mathbf{D}}{\partial t}\right)\cdot \mathbf{dA} \Rightarrow \mathbf{C}'\mathbf{u}_m = \mathbf{i} + \frac{\mathrm{d}\boldsymbol{\psi}}{\mathrm{d}t} \tag{16}$$

$$\hookrightarrow \operatorname{div}\mathbf{D} = \rho \quad \Rightarrow \quad \iint_{\Sigma} \mathbf{D}\cdot \mathbf{dA} = \iiint_{\mathcal{D}_\Sigma} \rho \,\mathrm{d}v \quad \Rightarrow \mathbf{D}\boldsymbol{\psi} = \mathbf{q} \tag{17}$$

$$\hookrightarrow \operatorname{div}\mathbf{J} = -\frac{\partial \rho}{\partial t} \quad \Rightarrow \quad \iint_{\Sigma} \mathbf{J}\cdot \mathbf{dA} = -\iiint_{\mathcal{D}_\Sigma} \frac{\partial \rho}{\partial t}\,\mathrm{d}v \quad \Rightarrow \mathbf{D}\mathbf{i} = -\frac{\mathrm{d}\mathbf{q}}{\mathrm{d}t} \tag{18}$$

FIT combines MGE with the Hodge's operators, which describe the material behavior

$$\begin{aligned} &\mathbf{B} = \mu\mathbf{H}, && \mathbf{D} = \varepsilon\mathbf{E}, && \mathbf{J} = \sigma\mathbf{E} && \Rightarrow \\ \Rightarrow \quad &\boldsymbol{\varphi} = \mathbf{M}_\mu \mathbf{u}_m = \mathbf{M}_\nu^{-1}\mathbf{u}_m, && \boldsymbol{\psi} = \mathbf{M}_\varepsilon \mathbf{u}_e, && \mathbf{i} = \mathbf{M}_\sigma \mathbf{u}_e. \end{aligned} \tag{19}$$

The main characteristics of the FIT method are:

- There is no discretization error in the MGE fundamental equations. All numerical errors are hold by the discrete Hodge operators.

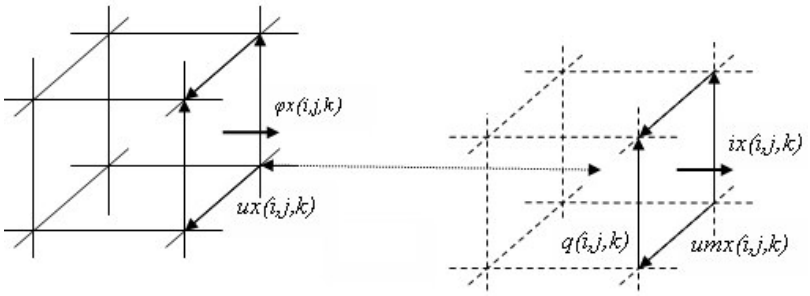

Fig. 3. Dofs for FIT numerical method in the two dual grids cells.

- An equivalent FIT circuit (Fig. 4), having MGE+Hodge as equations may be easily build. The graphs of the two constituent mutually coupled sub-circuits are exactly the two dual discretization grids; therefore the complexity of the equivalent circuit has a linear order with respect to the number of grid-cells [ICR06a].
- MGE are:
  - **sparse**, having maxim 6 non-zero entries per row,
  - **metric-free**: $\mathbf{C}$ - the discrete-curl and $\mathbf{D}$ - the discrete-div operators have only 0, +1 and -1 as entries,
  - **mimetic**: in Maxwell equations curl and div operators are replaced by their discrete counterparts $\mathbf{C}$ and $\mathbf{D}$, and
  - **conservative**: the discrete form of the discrete charge conservation equation is a direct consequence of both Maxwell and as well as of the MGE equations.

Due to these characteristics the numerical solutions have **no spurious modes**.

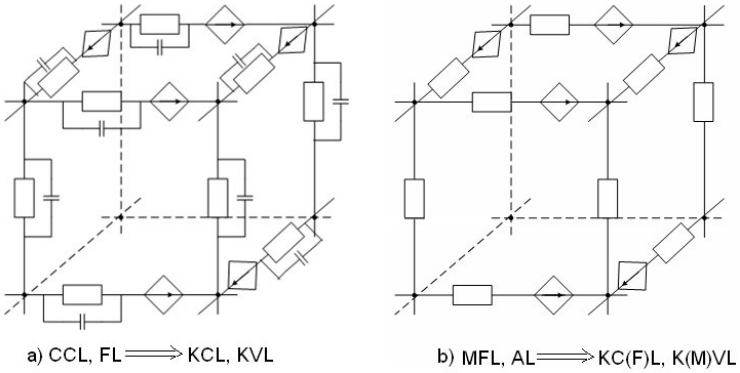

Fig. 4. Electric (left) and magnetic (right) equivalent FIT circuits.

The size of DOF vectors are:

- electric voltages $\mathbf{u}_e$ equal to the number of branches in the primary grid N_b;

- magnetic voltages $\mathbf{u}_m$ equal to the number of branches in the secondary grid N_b';
- magnetic fluxes $\boldsymbol{\varphi}$ equal to the number of faces in the primary grid N_f;
- electric fluxes $\boldsymbol{\psi}$ equal to the number of faces in the secondary grid N_f'.

In order to avoid confusions with the capacitance matrix $\mathbf{C}$ for the circuit in Fig. 4, in the rest of the paper the discrete-curl operator will be denoted by $\mathbf{B}$. Actually, it is the topological matrix of branches-loops incidence in the equivalent FIT electrical circuit, while the $\mathbf{B}'$ matrix is branches-loops incidence in the equivalent FIT magnetic circuit.

Details about how the elements of the matrices within MGE and Hodge operators can be computed and stored are presented for instance in [ICR06a]. As an example, typical expressions of Hodge operators are

$$M_{\sigma_{jk}} = \frac{1}{l_k} \sum_{j=1}^{4} \sigma_j A_j, \tag{20}$$

$$M_{\nu_{jk}} = \frac{1}{A_k} \sum_{j=1}^{2} \frac{l_j}{\mu_j}, \tag{21}$$

$$M_{\varepsilon_{jk}} = \frac{1}{l_k} \sum_{j=1}^{4} \varepsilon_j A_j, \tag{22}$$

where A is the area and l is the length, as they are represented in Fig. 5.

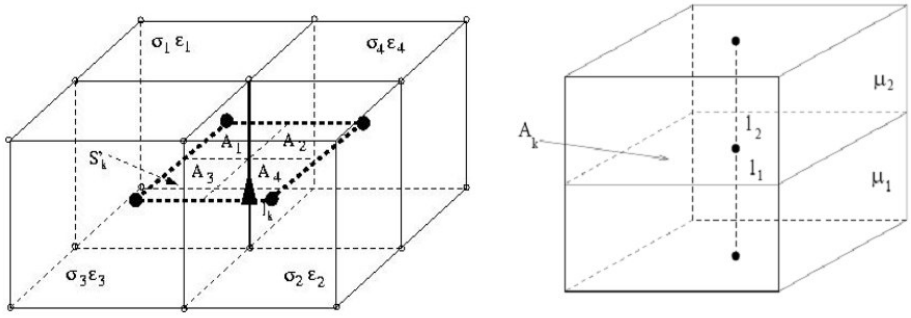

Fig. 5. Discretization of the Hodge operators.

Due to the fact that the elements of Hodge operators $\mathbf{M}_\sigma$, $\mathbf{M}_\nu$, $\mathbf{M}_\varepsilon$ have dimensions of electric conductance, magnetic reluctance and electric capacitance, they will be denoted by $\mathbf{G}_e$, $\mathbf{R}_m = \mathbf{G}_m^{-1}$, and $\mathbf{C}_e$, respectively. With these notations, the constitutive relationships become:

$$\boldsymbol{\varphi} = \mathbf{G}_m \mathbf{u}_m, \tag{23}$$

$$\boldsymbol{\psi} = \mathbf{C}_e \mathbf{u}_e, \tag{24}$$

$$\mathbf{i} = \mathbf{G}_e \mathbf{u}_e. \tag{25}$$

With these new notations, the MGE relationships (14) and (16) become:

$$\frac{\mathrm{d}\boldsymbol{\varphi}}{\mathrm{d}t} + \mathbf{B}\mathbf{u}_e = \mathbf{0}, \tag{26}$$

$$\frac{\mathrm{d}\boldsymbol{\psi}}{\mathrm{d}t} + \mathbf{i} - \mathbf{B}'\mathbf{u}_m = \mathbf{0}. \tag{27}$$

By eliminating the flux vectors, similar equations to the equations of an electric circuit are obtained:

$$\mathbf{G}_m \frac{\mathrm{d}\mathbf{u}_m}{\mathrm{d}t} + \mathbf{B}\mathbf{u}_e = \mathbf{0}, \tag{28}$$

$$\mathbf{C}_e \frac{\mathrm{d}\mathbf{u}_e}{\mathrm{d}t} + \mathbf{G}_e\mathbf{u}_e - \mathbf{B}'\mathbf{u}_m = \mathbf{0}, \tag{29}$$

with the following matrix representation:

$$\mathbf{C}\frac{\mathrm{d}\mathbf{x}}{\mathrm{d}t} + \mathbf{G}\mathbf{x} = \mathbf{0},$$
where
$$\mathbf{C} = \begin{bmatrix} \mathbf{G}_m & \mathbf{0} \\ \mathbf{0} & \mathbf{C}_e \end{bmatrix}, \quad \mathbf{G} = \begin{bmatrix} \mathbf{0} & \mathbf{B} \\ -\mathbf{B}' & \mathbf{G}_e \end{bmatrix}, \quad \mathbf{x} = \begin{bmatrix} \mathbf{u}_m \\ \mathbf{u}_e \end{bmatrix}. \tag{30}$$

The system (30) is very sparse, each row of the matrix $\mathbf{C}$ containing no more than one nonzero entry. By a suitable ordering of equations, the non-zero elements may be placed on the diagonal position of matrix, all non-diagonal elements being zero. The matrix $\mathbf{G}$ contains in each row no more than five nonzero elements: four with integer values (two +1 and two -1) and a real non-negative number.

The system (30) of DAE is far to be the complete I/O state-representation of our passive device, first of all, because the number of equations (E) is not equal to the number of variables (V). As a consequence, $\mathbf{C}$ and $\mathbf{G}$ are non-square matrices. The number of equations in (30) $E = N_f + N'_f$ is equal to the total number of elementary faces in both primary and secondary grids, while the number of variables $V = N_b + N'_b$ is equal to the total number of branches in both primary and secondary grids, therefore the size of both $\mathbf{C}$ and $\mathbf{G}$ matrices is $(N_f + N'_f) \times (N_b + N'_b)$ with $E < V$.

From the total number of electrical branches N_b, a number of N_{bB} branches are removed, corresponding to the branches placed on the boundary. The remaining number of $(N_b - N_{bB})$ branches is equal to the total number of the elementary magnetic faces. Meanwhile, to each magnetic branch corresponds an electric face, therefore without the electric boundary faces and branches, the number of equations $E' = (N_f - N_{fB} + N'_f)$ is equal to the number of state variables $V' = (N_b - N_{bB} + N'_b)$. Consequently, in this case, the deficit of equations in the system (30) is equal to the number of border branches N_{bB}. According to the Euler relation $N_{bB} = (N_{nB} - 1) + (N_{fB} - 1)$ is equal to the number of the boundary nodes excepting one plus the number of the boundary faces, excepting one. This deficit of equations $V' - E' = N_{bB}$ will be covered by the discrete form of the boundary

conditions. The FIT discretization of the Maxwell equations frequently described in literature does not explain the most difficult part of the algorithm, namely the set-up of the appropriate boundary conditions and their discretization, without which it is not possible to obtain a state space representation of the device, compatible with an external electric circuit, to which the device is connected.

3 State Representation of the Boundary Conditions

The first ECE boundary condition (8):

$$\mathbf{n} \cdot \operatorname{curl} \mathbf{E}(P,t) = \frac{\mathrm{d}B_n}{\mathrm{d}t} = 0 \quad \text{for } (\forall)\, P \in \Sigma, \tag{31}$$

is automatically satisfied when the normal component of the magnetic flux density is zero on the boundary. This happens naturally, because in our version of FIT there are no branches of the secondary (magnetic) grid crossing the boundary of the computational domain covered by the primary-electric grid. The discrete form of (31) is represented by the KVL written on the $(N_{fB}-1)$ boundary faces excepting one, where the KVL is a consequence. Therefore (30) keeps its form with both $\mathbf{C}$ and $\mathbf{G}$ matrices of size $(N_f + N'_f) \times (N_b + N'_b)$, but with zero values for $(N_{fB}-1)$ diagonal entries of $\mathbf{G}_m$.

The second ECE boundary condition (9):

$$\mathbf{n} \cdot \operatorname{curl} \mathbf{H}(P,t) = J_t = 0 \quad \text{for } (\forall)\, P \in S_e = \Sigma - \cup S'_k, \tag{32}$$

is satisfied when the normal component of the total current density (conduction plus displacement) is zero on the device boundary S_e, excepting on the device terminals. As a consequence, no current will be injected from outside:

$$i_k = 0, \quad \text{for any node } k \text{ on } S_e. \tag{33}$$

The third ECE boundary condition (10):

$$\mathbf{n} \times \mathbf{E}(P,t) = \mathbf{0} \qquad \text{for } (\forall)\, P \in S'_1, S'_2, \ldots, S'_n \tag{34}$$

is satisfied if the electric voltages along any terminal branches is zero:

$$u_{eb} = 0, \quad \text{for any branch } b \text{ belonging to any terminal } S'_k. \tag{35}$$

All equations associated to the faces placed on terminals can be eliminated, reducing the number of rows of matrices $\mathbf{C}$ and $\mathbf{G}$. The voltages $\mathbf{u}_{eb}$ (and the corresponding columns of matrices $\mathbf{C}$ and $\mathbf{G}$) can be eliminated from the set of the state variables as well.

For terminals excited in current, the non-homogeneous boundary condition can be expressed by means of Hodge operators as:

$$i_{Tk}(t) = \sum_{m \in S'_k} i_m = \sum_{m \in S'_k} \left(C_{e_m} \frac{\mathrm{d}u_{e_m}}{\mathrm{d}t} + G_{e_m} u_{e_m} \right), \tag{36}$$

where $i_{Tk}(t)$ is the total current injected in the terminal k. The sum is done over all electrical branches (belonging to the boundary or orthogonal to it) directly connected to the terminal k. The matrix representation of (36) is:

$$\mathbf{S}_C \frac{\mathrm{d}\mathbf{u}_e}{\mathrm{d}t} + \mathbf{S}_G \mathbf{u}_e = \mathbf{i}_T, \tag{37}$$

where $\mathbf{i}_T$ is the vector of the excitation currents injected in terminals. Denoting by $\mathbf{S}$, the branch-terminal connexion matrix (each row, associated to a terminal has elements of values +1 or -1 in the columns corresponding to branches connected to that terminal), we can write:

$$\mathbf{S}_C = \mathbf{S}\mathbf{C}'_e, \quad \mathbf{S}_G = \mathbf{S}\mathbf{G}'_e, \tag{38}$$

where $\mathbf{C}'_e$ and $\mathbf{G}'_e$ are square diagonal matrices of Hodge operators, with the size equal to the total number of primary branches including those on boundary (size of $\mathbf{u}_e$).

The boundary condition (33), can be written as (36) with zero left hand side. This is equivalent to the extension of the matrix $\mathbf{S}$, by adding a row for any node on the boundary surface (excepting for the terminals). In this manner, the Kirchhoff current law on all boundary nodes is imposed, excepting for the reference node, for which KCL is a consequence. 0 By combining (30) with the boundary conditions (37) the semi-state descriptor representation of the system associated to the passive integrated component is obtained:

$$\mathbf{C} \frac{\mathrm{d}\mathbf{x}}{\mathrm{d}t} + \mathbf{G}\mathbf{x} = \mathbf{w}, \tag{39}$$

where

$$\mathbf{C} = \begin{bmatrix} \mathbf{G}_m & \mathbf{0} \\ \mathbf{0} & \mathbf{C}_e \\ \mathbf{0} & \mathbf{S}_C \end{bmatrix}, \quad \mathbf{G} = \begin{bmatrix} \mathbf{0} & \mathbf{B} \\ -\mathbf{B}' & \mathbf{G}_e \\ \mathbf{0} & \mathbf{S}_G \end{bmatrix}, \quad \mathbf{w} = \begin{bmatrix} \mathbf{0} \\ \mathbf{0} \\ \mathbf{i}_T \end{bmatrix} = \mathbf{B}_i \mathbf{i}_T, \tag{40}$$

with $\mathbf{C}$ and $\mathbf{G}$ square matrices and $\mathbf{i}_T$ as the input vector of terminal excitation currents. If instead of KCL (36) for the boundary nodes, the nodal equations (or the equations of the tree voltages) are used, then the $\mathbf{C}$ matrix becomes a symmetric positive definite one (and the state space becomes a minimal one).

In this final form of state equations, the following relaionships are also embedded as it expected: the constitutive relations of all electric and magnetic branches, Faraday and Ampere-Maxwell laws over all mesh-grid, Kirchhoff voltage and current/flux laws in all nodes (in internal nodes as a consequence) and finally, the terminal excitation conditions.

If all floating **terminals of the device are current-excited**, then the output signals are the electrical voltages of terminals:

$$u_{Tk} = \sum_{m \in C_k} u_{em}, \tag{41}$$

where C_k is a set of branches which compose a path from the current terminal k to the reference terminal. The matrix form of (41) is

$$\mathbf{u}_T = \mathbf{S}_u \mathbf{u}_e, \tag{42}$$

where $\mathbf{u}_T$ is the system response and $\mathbf{S}_u$ is the branch-to-path connection matrix (+1 or -1 for boundary branches comprising the path). In conclusion, in the current-excitation case, the complete LTI system is defined by semi-state equations (39) and the output relations (42):

$$\begin{aligned} \mathbf{C}\frac{\mathrm{d}\mathbf{x}}{\mathrm{d}t} + \mathbf{G}\mathbf{x} &= \mathbf{B}_i \mathbf{i}_T, \\ \mathbf{u}_T &= \mathbf{S}_u \mathbf{u}_e, \end{aligned} \tag{43}$$

with $\mathbf{C}$ and $\mathbf{G}$ given by (40). The transfer function of the MIMO system (43) is the impedance matrix $\mathbf{Z}$ of the passive component.

In the case of **voltage-excited components**, (37) may describe the output and (41) may describe the input relationships. However, there is still another representation of the voltage-excited device, as a standard LTI system, without time derivative in the output equations. It is generated by the definition (11) of the terminal current. The discrete form of this relationship is:

$$i_{Tk}(t) = \sum_{m \in \Gamma_k} u_{em} \tag{44}$$

where Γ_k is a set of branches defining the contour of the terminal k. The matrix form of (44) is

$$\mathbf{i}_T = \mathbf{S}_i \mathbf{u}_e, \tag{45}$$

where $\mathbf{i}_T$ is the vector of response currents and $\mathbf{S}_i$ is the branch-to-contours connection matrix (+1 or -1 for boundary branches comprising the contour). In conclusion, when all device terminals are voltage-controlled, the complete LTI system can be defined alternatively by the semi-state equations (39) with $\mathbf{w} = \mathbf{B}_u \mathbf{u}_T$ and the output relations (45):

$$\begin{aligned} \mathbf{C}\frac{\mathrm{d}\mathbf{x}}{\mathrm{d}t} + \mathbf{G}\mathbf{x} &= \mathbf{B}_u \mathbf{u}_T, \\ \mathbf{i}_T &= \mathbf{S}_i \mathbf{u}_e, \end{aligned} \tag{46}$$

with $\mathbf{C}$ and $\mathbf{G}$ given by (40), $\mathbf{u}_T$ the vector of excitation voltages and $\mathbf{i}_T$ the response vector of terminal currents. The transfer function of the MIMO system (46) is the admittance matrix $\mathbf{Y}$ of the device.

If the **component is hybrid excited**, the associated LTI system is defined by:

$$\begin{aligned} \mathbf{C}\frac{\mathrm{d}\mathbf{x}}{\mathrm{d}t} + \mathbf{G}\mathbf{x} &= \mathbf{B}'\mathbf{w}, \\ \mathbf{y} &= \mathbf{L}\mathbf{x}, \end{aligned} \tag{47}$$

with

$$\mathbf{x}=\begin{bmatrix}\mathbf{u}_m\\ \mathbf{u}_e\end{bmatrix},\mathbf{w}=\begin{bmatrix}\mathbf{u}_T{}'\\ \mathbf{i}_T{}''\end{bmatrix},\mathbf{B}'=\begin{bmatrix}\mathbf{B}'_u & \mathbf{0}\\ \mathbf{0} & \mathbf{B}'_i\end{bmatrix},\mathbf{y}=\begin{bmatrix}\mathbf{i}'_T\\ \mathbf{u}_T{}''\end{bmatrix},\mathbf{L}=\begin{bmatrix}\mathbf{S}_i & \mathbf{0}\\ \mathbf{0} & \mathbf{S}_v\end{bmatrix}, \quad (48)$$

where the matrices $\mathbf{C}$, $\mathbf{G}$, $\mathbf{B}'$, $\mathbf{L}$, input vector $\mathbf{w}$ and output vector $\mathbf{y}$ are defined accordingly, by combining (43) and (46). Regardless the excitation mode, the state variables are the voltages along the all electric and magnetic grid branches, excepting those on terminals. The transfer function of the MIMO system (47) is the hybrid matrix $\mathbf{H}$ of the passive component:

$$\begin{aligned}&\mathbf{y}=\mathbf{H}\mathbf{w}=\mathbf{L}\mathbf{x}=\mathbf{L}\left(s\mathbf{C}+\mathbf{G}\right)^{-1}\mathbf{B}'\mathbf{w} \quad \Rightarrow\\ \Rightarrow \quad &\mathbf{H}=\mathbf{L}\left(s\mathbf{C}+\mathbf{G}\right)^{-1}\mathbf{B}'.\end{aligned} \quad (49)$$

If the first m out of total n terminals are controlled in voltage and the rest $n-m$ are controlled in current, the hybrid matrix has the following block structure:

$$\mathbf{H}=\begin{bmatrix}\mathbf{H}_{11} & \mathbf{H}_{12}\\ \mathbf{H}_{21} & \mathbf{H}_{22}\end{bmatrix},\mathbf{y}=\mathbf{H}\mathbf{w}=\begin{bmatrix}\mathbf{i}_T{}'\\ \mathbf{u}_T{}''\end{bmatrix}=\begin{bmatrix}\mathbf{H}_{11} & \mathbf{H}_{12}\\ \mathbf{H}_{21} & \mathbf{H}_{22}\end{bmatrix}\begin{bmatrix}\mathbf{u}_T{}'\\ \mathbf{i}_T{}''\end{bmatrix} \quad (50)$$

where $\mathbf{H}_{11}=\mathbf{Y}$ is the square admittance matrix of size m, $\mathbf{H}_{22}=\mathbf{Z}$ the square impedance matrix of size $(n-m-1)$, while $\mathbf{H}_{12}$ is the voltage transfer coefficient and $\mathbf{H}_{21}$ is the current transfer coefficient. In the degenerate case, when $m=0$, the matrix $\mathbf{H}$ becomes the impedance matrix, and when $m=n-1$, then $\mathbf{H}$ becomes the admittance matrix of the component. The number of inputs is equal to the number of outputs. Each device terminal, excepting the reference terminal has either its voltage or its current as an input scalar signal, and its current and respectively its voltage as an output.

4 ROM WorkBench

The next step after the extraction of the state space model for passive components is the order reduction. In order to decide which ROM technique is the most appropriate for this type of model, a new tool called *ROM Workbench* was conceived in the frame of the FP6/IST/CODESTAR project [webb]. Its aim is to allow the user to reduce models by means of as many ROM techniques as possible, and to compare the results. The ROM Workbench consists of a set of benchmark problems, a set of model order reduction methods and criteria for results evaluation and comparison. Fig. 6 shows the main blocks of the ROM Workbench. The models that can be read in are of various types: linear time invariant systems given by state (or semi-state) space matrices, frequency responses described by the variation of impedance, admittance or scattering parameters with respect to the frequency, circuits given as net-lists or transfer functions given by poles and residues. Once read into the database of models, different actions can be carried out. The most important is the reduction but other actions are also useful, such as conversions between different types of representations,

characterization/visualization of a system (plots or computation of lumped or line parameters, etc), or synthesis of the equivalent circuit. A very important facility is that the systems can be compared, the comparison between the original model and reduced models obtained from different reduction techniques allowing one to decide which method performs best for a given problem.

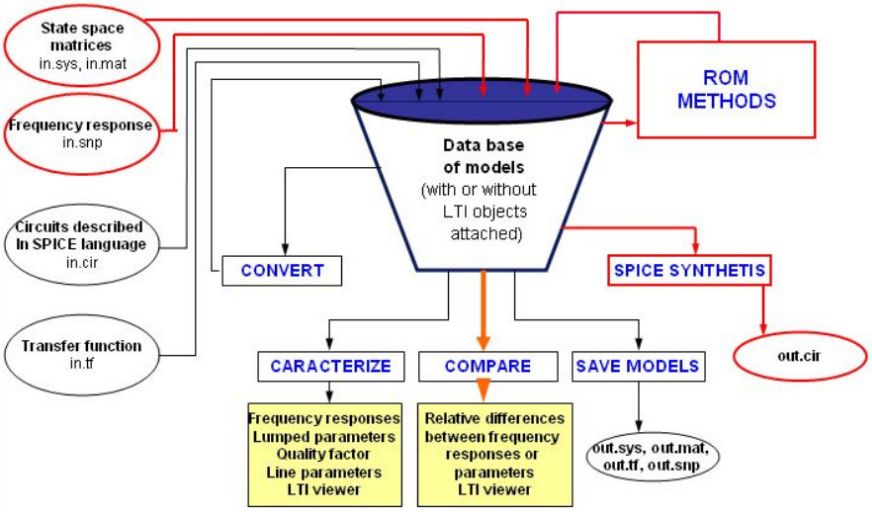

Fig. 6. Main blocks of the ROM Workbench.

The reduction can be carried out by means of various methods. These methods include: explicit moment matching, Krylov subspace techniques [CPO02], Laguerre techniques [KZ99], combined techniques (such as two step Lanczos, or Krylov based followed by a truncated balanced reduction), and truncated balanced realization procedures [webc]. The vector fitting method proposed in [GS99], which finds the transfer function matching a given frequency characteristic is included in the ROM Workbench as an order reduction method.

The workbench is able to compare responses obtained for different systems. The comparison can be carried out either on the time responses (step, impulse, etc.) or on the frequency responses (Bode, Nyquist, Smith, etc). Lumped parameters, quality factors or line parameters can also be compared.

The available measurements data for the tested devices are usually the scattering ($\mathbf{S}$) parameters. That is why, in the results that follows the criteria used for comparison is an error estimator based on the Frobenius norm $||.||_F$, computed as $\text{rms}||\mathbf{S}_{\text{ref}} - \mathbf{S}_{\text{an}}||_F / \max_f ||\mathbf{S}_{\text{ref}}||_F$, where $\mathbf{S}_{\text{ref}}$ are the scattering parameters for the reference system (for instance the measured data), and $\mathbf{S}_{an}$ are the scattering parameters of the analyzed system, for instance the reduced order model.

The first implementation of the ROM workbench was under Matlab, with GUI. This implementation proved to be very useful, as a prototyping tool in the re-

search as well as for the educational purposes (see for instance the MOR course `http://www.win.tue.nl/casa/meetings/special/mor/`). Other implementations do not use any graphical interface at all, being appropriate for linking the reduction step to the EM simulator, especially in the case of large scale problems that need high computational resources. For instance, in the CODESTAR project various tools of the ROM Workbench became stand alone programs using the MATLAB Compiler Toolbox. Future versions of the ROM Workbench will include features related to parameterization, its further development being supported in the frame of the CHAMELEON-RF project [weba].

5 All Levels Reduced Order Modelling

The ROM WorkBench procedures were applied to a series of test structures, relevant to the Codestar project, which will be described in the next section. The reduced order method which behaved best in these study cases was the one based on Vector Fitting [GS99]. Another important conclusion of the numerical experiments was that *a-posteriori* order reduction is not enough effective, if it is not accompanied by *a-priori* and *on-the-fly* reduced order techniques. The idea to apply any reduction as soon as possible in the model extraction process lead to a strategy called **ALROM - All Levels Reduced Order Modeling** [ICRS06], which basically uses the following steps to model the passive components and interconnects:

A) Grid calibration. The minimal orthogonal grid necessary to define the material sub-domains is successively refined, until the equivalent capacitances of the passive component are accurate enough. The **dual Finite Integration Technique (dFIT)** used to solve the electrostatic field equations and to extract the capacitances provides lower and upper bounds of the exact solution [IRC04]. These bounds are used to control the accuracy of the numerical solution by means of a multi-grid approach.

B) Virtual boundary calibration. The computational domain is successively extended, until the inductance extracted by averaging the dual Neumann and Dirichlet boundary conditions is accurate enough [ICR06b]. Actually, an Equivalent Layer on the boundary of the computational domain is used to model the Open Boundary of the magneto-static field. Choosing for the material constant of ELOB (Equivalent Layer of Open Boundary) the magnetic relative permeability $\mu_r \ll 1$, the scalar magnetic potential satisfies the Neumann boundary condition, while for $\mu_r = M \gg 1$ the potential satisfies the Dirichlet boundary condition. These two dual boundary conditions are used to control the accuracy of the numerical solution because they provide lower and upper bounds of the inductances extracted from the exact field solution in the un-bounded domain.

C) Frequency analysis. By using the grid resulted in previous steps, after refining and extension process, the frequency dependent matrix of the component is computed in a minimal set of frequency samples, solving the linear complex system (49), a FIT consequence of Maxwell equations. To build numerical scissors for the exact solution, a practical approach we propose is to use the dual (complementary)

solutions, solving the Maxwell Grid Equations two times, and computing the admittance matrix using the two dual-staggered grids and two type of boundary conditions, for a sequence of frequency samples ω:

- $\mathbf{Y}_p(\omega)$ is computed by FIT on the primary grid with ELOB parameters $\varepsilon_r = M \gg 1$, $\mu_r = 1$;
- $\mathbf{Y}_s(\omega)$ is computed by FIT on the secondary grid with ELOB parameters $\varepsilon_r = 1$, $\mu_r = M \gg 1$.

By averaging the two admittance, a numerical solution $\mathbf{Y}_a(\omega) = (\mathbf{Y}_p(\omega) + \mathbf{Y}_s(\omega))/2$ is generated, which provides a better accuracy than any of the two direct extracted admittances $\mathbf{Y}_p(\omega)$ or $\mathbf{Y}_s(\omega)$, at least at low frequencies. In the case of interconnects, the p.u.l. frequency dependent line parameters $\mathbf{Z}_l(\omega) = \mathbf{R}_l(\omega) + j\mathbf{L}_l(\omega)$ and $\mathbf{Y}_l(\omega) = \mathbf{G}_l(\omega) + j\mathbf{C}_l(\omega)$ are extracted using a similar technique, but solving the 2D EMQS equation of the TM field [ICRS06].

D) Length extension. This is an optional step, applied in the case of the TL model for interconnects. The frequency characteristic $\mathbf{Y}(\omega)$ of the real length line is computed by transmission line equations in an extended set of adaptive frequency samples, using an appropriate interpolation of p.u.l. parameters.

E) Optimal order of the compact model. In this algorithm step, the frequency characteristic $\mathbf{Y}(\omega)$ of the analyzed component is approximated by rational functions using the Vector Fitting procedure [GS99] and then a SPICE equivalent circuit is synthesized by the Differential Equation Macromodel [PR04]. The couple of these procedures is iterated, successively increasing the order of the extracted model. Compact models of increasing order and their equivalent circuits are extracted and simulated in the frequency domain with SPICE, until the result is close to $\mathbf{Y}(\omega)$, on the frequency range of interest. In this way, the compact model and its SPICE equivalent circuit for the given components having an optimal order are generated.

F) Validation. Based on the results of the SPICE simulation in frequency domain, the scattering parameters $\mathbf{S}(\omega)$ are computed and compared with the measurements, for a series of test structures, of practical interest - the Codestar benchmarks, presented below.

The control of the solution accuracy plays a crucial role in *a-priori* order reduction. Use of an optimal grid minimizes the number of required DOFs. By extending or refining more the optimal grid, the order of the macro-model generated by discretization is increased, whereas by reducing the grid size the solution accuracy becomes too low to be acceptable.

6 Test Structures

6.1 Meander resistor (RPOLY2_ME benchmark)

A semi-state space model for the meander on-chip resistor depicted in Fig. 7 has been computed using the finite integration technique described above. For a grid having 368200 nodes, a macro-model having 19510 degrees of freedom has been obtained using a-priori order reduction techniques.

After the computation of its frequency response on the range 1-20 GHz, a reduced order model of order four was obtained using the vector fitting algorithm. This reduced model was then synthesized and the equivalent circuit thus obtained has been simulated with SPICE. The relative error of $\mathbf{S}$ parameters between the simulation of the initial model and the reduced one is very low, about 0.16 %. The reduction time was also very low, less than 1 second. Fig. 8 shows the relative error between the macromodel and the reduced model for increasing order of the reduced system. Even for very low orders, vector fitting was able to find accurate reduced models.

Fig. 9 shows the comparison between the measurements (real part of parameter S_{11}) and the simulation of the reduced order model. Fig. 10 shows the same comparison for the extracted resistance.

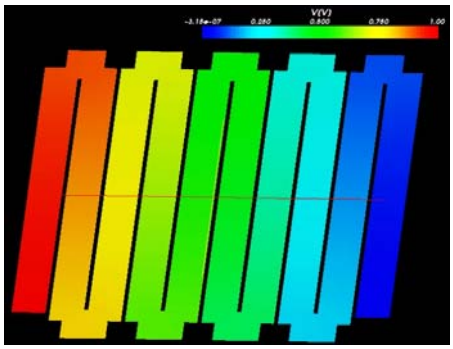

Fig. 7. Meander resistor benchmark.

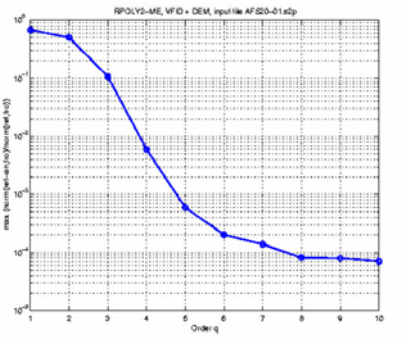

Fig. 8. Relative error versus the order of the reduced system.

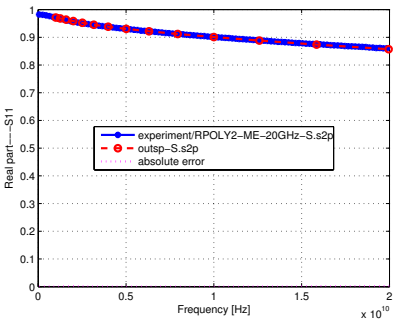

Fig. 9. Parameter S_{11} - measurement and simulation of reduced model.

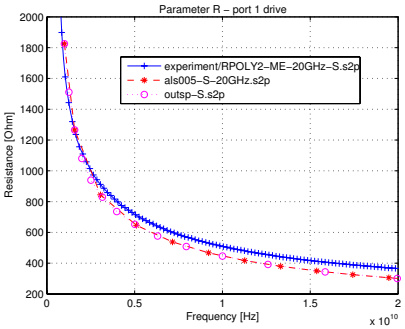

Fig. 10. Rezistence extracted from measurements, simulation of initial and reduced models.

6.2 Capacitor (CMIM benchmark))

Another benchmark tested was a metal-insulator-metal capacitor (Fig. 11). A grid having 833280 nodes have been used, conducing to a macro-model of order 29925. The macro-model has been reduced to a model of order four, using the vector-fitting algorithm. The relative error between the initial model and the reduced one is 0.2 %, obtained in less than 1 second. The relative error between the measurements and the reduced model is 3.75 %.

Figs. 13 and 14 show the comparison between measurements (S_{12} real and imaginary parts) and simulation of reduced model. Fig. 12 shows the variation of the extracted capacitance with respect to the frequency.

6.3 SP-SMALL benchmark

In the case of an inductor benchmark (Fig. 15), a grid having 596068 nodes generates a macro-model of order 9614. This has been reduced also to a model of order four, using the vector-fitting algorithm. The relative error between the initial model and the reduced one is 0.5 %, obtained in less than 1 second. Figs. 17 and 18 show the comparison between the macro-model frequency response (S_{11} real and imaginary parts) and simulation of reduced model. Fig. 16 shows the variation of the extracted inductance with respect to the frequency.

6.4 Coplanar Line

A coplanar line discretized with a grid having 2866441 nodes generates a macro-model of order 19972. The vector-fitting procedure was also the most successful reduction procedure for this case, generating a reduced order model with ten degrees of freedom, in less than 1 second. The error between the initial macro-model and the reduced model is 1.3 %, for a frequency range 1-30 GHz. This corresponds to a relative error between measurements and reduced order model of 5.5 %. Fig. 19

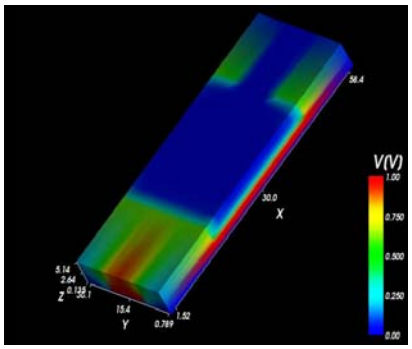

Fig. 11. Capacitor benchmark.

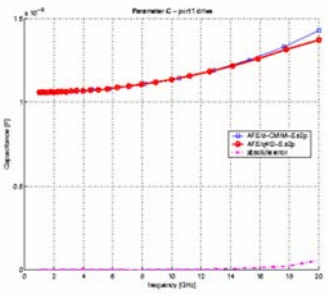

Fig. 12. Capacitance extracted from the simulation of initial model and of reduced model.

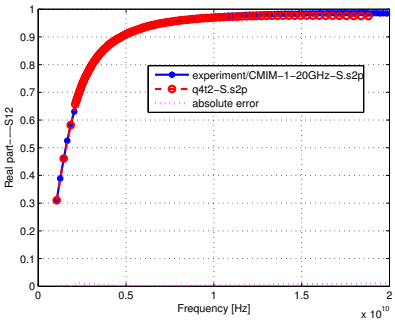

Fig. 13. Parameter S_{12} - real part, experiment and reduced model.

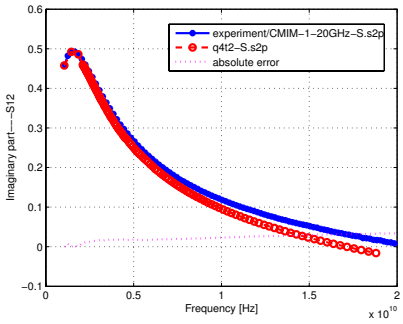

Fig. 14. Parameter S_{12} - imaginary part, experiment and reduced model.

shows how the order increasing improves frequency response of the reduced order model.

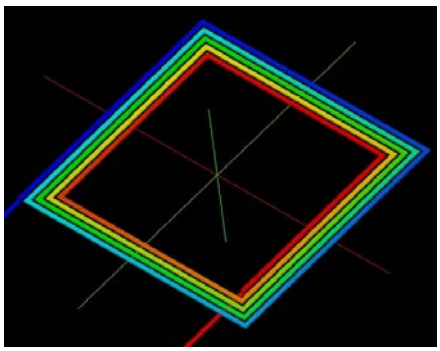

Fig. 15. Inductor benchmark.

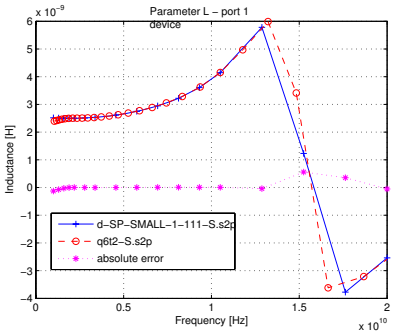

Fig. 16. Extracted inductance: simulation of macromodel and reduced model.

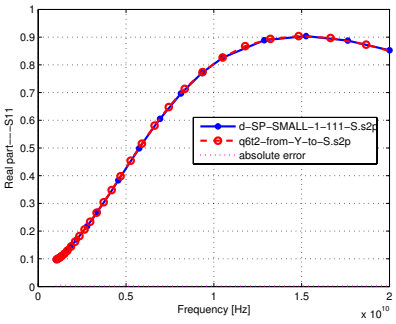

Fig. 17. Parameter S_{11} - real part.

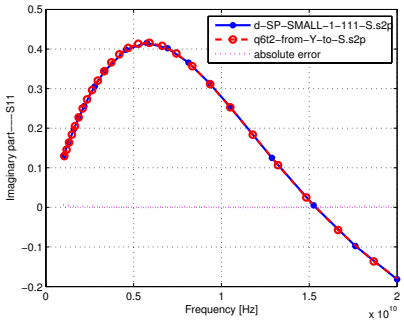

Fig. 18. Parameter S_{11} - imaginary part.

Files corresponding to these four benchmarks (macromodels, reduced order models and the measured frequency characteristics) may be found at `www.lmn.pub.ro/~codestar`.

7 Conclusions

The proposed strategy proved to be an efficient methodology for modeling and simulation of on-chip passive components.

An important step in the modeling process is represented by the correct formulation of the EM field problem in mathematical terms. The proper boundary conditions and the solution uniqueness theorem allow the consistent definition of a dynamical system with distributed parameters. The next step is to reduce the system space-state at a finite dimension, applying a numerical method. FIT was the numerical method suitable for the class of integrated passive components. In order to extract the models for these components as state-space representations the discrete form of the boundary conditions plays a crucial role. The electric and magnetic voltages along the edges of the dual FIT grids are the state variables of the model.

When applying reduction procedures for a given model, an environment such as the ROM Workbench is very useful due to its flexibility. It allowed us to conclude that the vector fitting procedure is the best method to reduce electromagnetic full-wave models of passive components considered as Codestar benchmarks. For this class of problems, the reduction conduces to very low orders (less than 10) with an extremely low computational effort (less than 1 sec), the relative error between the simulation result and its reduced order model being less than 1

Acknowledgment

The authors would like to acknowledge the support of Ehrenfried Seebacher (Austriamicrosystems) for providing, within the common European Codestar research project [webb], the experimental data used in this paper.

References

[CPO02] Mustafa Celik, Lawrence Pileggi, and Altan Odabasioglu. *IC Interconnect Analysis*. Kluwer Academic Publishers, 2002.

[CW01] M. Clemens and T. Weiland. Discrete electromagnetism with the finite integration technique. *Progress in Electromagnetics Research (PIER)*, 32:65–87, 2001. http://ceta.mit.edu/PIER/pier.php?volume=32.

[GS99] B. Gustavsen and A. Semlyen. Rational approximation of frequency domain responses by vector fitting. *IEEE Trans. Power Delivery*, 14(3):1052–1061, 1999.

[ICR06a] D. Ioan, G. Ciuprina, and M. Rădulescu. Algebraic sparsefied partial equivalent electric circuit - aspeec. *Scientific Computing in Electrical Engineering (A.M. Anile, G. Al and G. Mascali Eds*, 9:45–50, 2006.

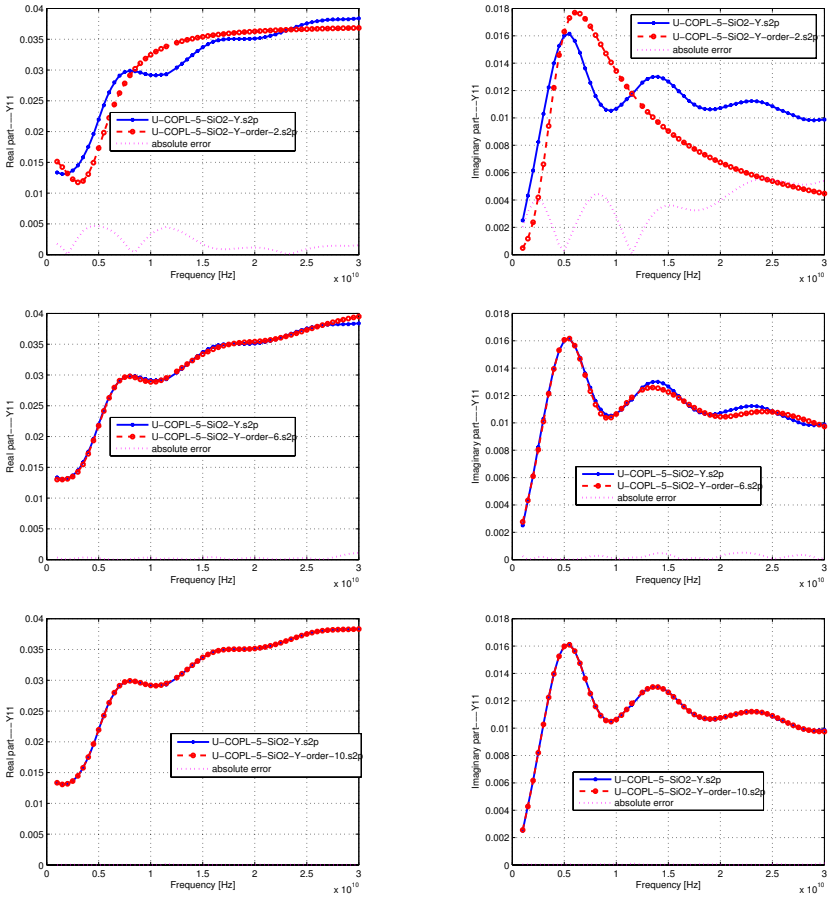

Fig. 19. Comparison between measurements (admittance) and reduced order model: left figures: real parts for measurements and reduced models of order (from top to bottom) 2, 6, 10; right figures - similar for imaginary parts.

[ICR06b] Daniel Ioan, Gabriela Ciuprina, and Marius Rădulescu. Absorbing boundary conditions for compact modeling of on-chip passive structures. *COMPEL: The International Journal for Computation and Mathematics in Electrical and Electronic Engineering*, 25(3):652–659, 2006.

[ICRS06] D. Ioan, G. Ciuprina, M. Rădulescu, and E. Seebacher. Compact modeling and fast simulation of on-chip interconnect lines. *IEEE Transactions of Magnetics*, 42(4):547–550, 2006.

[IM99] D. Ioan and I. Munteanu. Missing link rediscovered: The electromagnetic circuit element concept. *JSAEM Studies in Applied Electromagnetics and Mechanics*, 8:302–320, 1999.

[IRC04] D. Ioan, M. Rădulescu, and G. Ciuprina. Fast extraction of static electric parameters with accuracy control. *Scientific Computing in Electrical Engineering*, 4:248–256,

2004.

[KZ99] L. Knockaert and D. De Zutter. Laguerre-svd reduced order modeling. *Electrical Performance of Electronic Packaging*, pages 249–252, 1999.

[PR04] T. Palenius and J. Roos. Comparison of reduced-order interconnect macromodels for time-domain simulation. *IEEE Trans. Microwave Theory and Techniques*, 52(9):2240–2250, 2004.

[RTT66] R. Răduleţ, A. Timotin, and A. Tugulea. Introduction des parametres transitoires dans l'tude des circuits electrique lineaires ayant des elements non filiformes et avec pertes suplimentaires. *Rev. Roum. Sci Techn. - Electrotech. et Energ.*, 11(4):565–639, 1966.

[weba] CHAMELEON-RF website. www.chameleon-rf.org.

[webb] CODESTAR website. www.imec.be/codestar.

[webc] SLICOT website. The control and systems library slicot, www.slicot.com.